Stability analyses for deviated wellbores in unconsolidated cross-anisotropic formations

Citation: Akl, Sherif A.Y., and Andrew J. Whittle. "Stability Analyses for Deviated Wellbores in Unconsolidated Cross-Anisotropic Formations." Canadian Geotechnical Journal 53, no. 9 (September 2016): 1450–1459.

As Published: http://dx.doi.org/10.1139/CGJ-2015-0456

Publisher: Canadian Science Publishing

Persistent URL: http://hdl.handle.net/1721.1/117550

Version: Author's final manuscript: final author's manuscript post peer review, without publisher's formatting or copy editing

STABILITY ANALYSES FOR DEVIATED WELLBORES IN UNCONSOLIDATED CROSS-ANISOTROPIC FORMATIONS

Sherif A. Y. Akl

Assistant Professor, Soil Mechanics and Foundations Research Laboratory, Cairo University, Egypt.

Andrew J. Whittle

Edmund K. Turner Professor of Civil and Environmental Engineering, MIT, Cambridge, MA.

Corresponding and First Author

Dr. Sherif A. Akl

Assistant Professor

Soil Mechanics and Foundations Research Laboratory

Faculty of Engineering, Cairo University

1 Elgamaa Street

Giza 12316

Egypt

Phone: +2 0106 138 8880

Email: sherif.akl@cu.edu.eg, saakl@alum.mit.edu

Coauthor:

Dr. Andrew J. Whittle

Edmund K. Turner Professor of Civil Engineering

Massachusetts Institute of Technology

Room 1-346

77 Massachusetts Avenue

Cambridge, MA, 02139

Telephone: 617.253.7122

Email: ajwhittl@mit.edu

ABSTRACT

Production of oil from shallow reservoirs typically involves drilling highly deviated wells through unconsolidated (or poorly lithified) rocks or clays. This paper describes numerical analyses of the deformations and stability of deviated wellbores within a K_0-consolidated clay. The analyses consider planar deformations in the plane orthogonal to the wellbore using a quasi-3D finite element model that represents coupled flow and deformations within the soil mass. Cross-anisotropic mechanical properties of the clay are described by a generalized effective stress model, MIT-E3, with parameters previously calibrated from laboratory thick-walled cylinder tests. The analyses compute the relationship between the drilling mud pressure and wellbore stability associated with either the onset of localized failure mechanisms or large plastic deformations around the cavity. The results show that short-term, undrained stability requires mud pressures in excess of the in-situ formation pore pressures for more highly deviated wellbores at inclinations greater than 45^0. The analyses examine the mechanisms for further destabilization, due to consolidation within the formation, and how they are affected by drainage conditions at the wellbore wall. The results provide qualitative information for the design and control of drilling operations for deviated wellbores in unconsolidated formations.

KEYWORDS:

Numerical Analysis, wellbore stability, constitutive model, clay behavior, coupled analysis.

INTRODUCTION

In the ever expanding search for new sources of oil and gas, the industry is investigating new prospects in very shallow reservoirs (depths less than 1000m) including deep water sites in the Gulf of Mexico and onshore sites in the North Slope of Alaska. The effective exploitation of such reservoirs depends on a small number of surface drilling locations, with highly deviated wells and complex directional trajectories. The formations encountered at such shallow depths are poorly-lithified and are more properly classified as unconsolidated rocks or stiff clays. These materials have much lower shear strength than deeper reservoir rocks, exhibit highly non-linear deformation properties, are strongly anisotropic and can exhibit strain-softening in some modes of shearing. Typical wellbores pass vertically through the weaker upper sediments and are cased and cemented to mitigate effects of near-surface disturbance. Hence, wellbore stability methods commonly employed in the design of deep wells are based on assumptions appropriate to the strength and deformation characteristics of well-lithified rock formations. These methods depend on a proper determination of the drilling fluid density that provides pressure inside the cavity of the wellbore. In order to prevent influx of fluid, it is necessary to keep the mud pressure above the pore pressure at the cavity wall. Underbalanced drilling refers to situations where the mud pressure is less than the pore pressure. Fjaer et al (2008) divided instabilities into two categories of wellbore failures based on the type of mobilized strength, compressive or tensile failure: Compressive failure is caused by insufficient mud pressure leading to stress concentrations that exceed the rock strength; while tensile failure occurs when mud pressure exceeds the minor principal stress in the formation. These two constraints define the minimum and maximum mud weights usually associated with stable drilling.

For boreholes drilled entirely within unconsolidated rocks, drilling operations can be affected by significant squeezing associated with plastic deformations in the formation. Given the complexity of soil behavior, reliable predictions of borehole deformations and stability can only be achieved by relatively sophisticated constitutive models that are able to represent realistically the anisotropic stress-strain-strength properties of these clay and shale formations.

This paper presents numerical analyses for prototype vertical and deviated wellbores in these ductile formations. Mechanical properties of the clay are represented by generalized effective stress soil models calibrated to elemental tests on Resedimented Boston Blue Clay (RBBC), an analog shale material. Akl and Whittle (2016) have also validated predictions of the models using results of Thick Walled Cylinder (TWC) tests performed on the same material by Abdulhadi et al. (2011).

The analyses use quasi-3D models of directional wellbores to simulate effective stresses and pore pressures coupled deformations and flow around the wellbores. We initially focus on the prediction of instabilities due to short-term, undrained shearing of the clay as a function of the wellbore orientation, and then consider how fluid migration and coupled consolidation can contribute to further instability.

NUMERICAL MODEL

The axial dimension of the wellbore is characteristically several orders of magnitude larger than its in-plane dimensions (i.e. diameter is O [1m] while depth is O [10^3m]). Hence, it is appropriate to assume plane strain geometry for the wellbore model. Similarly, gradients of the gravitational forces are small compared to stress changes in the cross-sectional planes of interest

and can be ignored. These two assumptions lead to the popular plane strain wellbore model as discussed by Santarelli et al. (1986), Detournay and Cheng (1988); and Charlez and Hugas (1991).

The current analyses make the key assumption that the formation comprises 1-D consolidated sediments, such that far field stresses, in the global frame of reference, are fully defined by the effective vertical overburden stress, σ'_{v0}, and the lateral earth pressure ratio, K_0, associated with the consolidation stress history. Stress conditions in the horizontal (x-y) plane are isotropic (i.e, $\sigma'_{xx} = \sigma'_{yy} = K_0\sigma'_{v0}$). Mechanical (deformation and strength) properties of the formation are also expected to be isotropic for shearing in the horizontal plane (i.e. the material has circular symmetry and cross-anisotropic properties). These conditions are strictly only applicable for horizontally-layered sediments with a level ground surface.

The wellbore orientation is defined by the deviation and azimuthal angles. For wellbores installed in K_0-consolidated formations, behavior is fully defined by the deviation angle, ω, Figure 1a, with respect to the global frame of reference (X, Y, Z). Figure 1b illustrates a cross-section perpendicular to the wellbore axis (i.e, local frame of reference [x, y, z]). Wellbore deviation ($\omega \neq 0^0$) results in an out-of-plane shear component, σ_{yz}. Figure 2a shows the 'slice model' used to approximate the far field stresses and plane strain boundary conditions in a half space cross-section orthogonal to the wellbore axis (z), where the y-axis is an axis of symmetry (approximating complementary shear stresses in the axis of the wellbore). The slice model has a limited thickness in the z-direction (single layer of 3D elements) to accommodate out-of-plane shear components from the geostatic stress tensor.

The quasi-3D problem geometry reverts to a 2D (plane strain) problem only for special cases corresponding to vertical ($\omega = 0^0$) and horizontal ($\omega=90^0$) wellbores. For these 2D situations the

wellbore stability can be analyzed using a plane strain analysis of the quarter plane model as shown in Figure 2b. For a vertical wellbore ($\omega = 0^0$), the far field stresses are isotropic ($\sigma'_{yy} = \sigma'_{xx} = \sigma'_{h0} = K_0\sigma'_{v0}$) while the horizontal case ($\omega = 90^0$) introduces far field deviatoric stress conditions ($\sigma'_{yy} = \sigma'_{v0}$ and $\sigma'_{xx} = K_0\sigma'_{v0} = \sigma'_{h0}$). Far field stresses in the local and global frames of reference are calculated through standard transformation of tensors (Appendix A).

The current analyses were performed using the commercial finite element program ABAQUS^{TM} (Version 6.7; Hibbett et al. 1998). The mesh consists of mixed elements (displacement and pore pressure degrees of freedom). Figure 3 shows the finite element mesh for the quasi-3D 'slice' problem. The mesh uses a single layer of 1658 brick elements with quadratic interpolation of displacements and linear interpolation of pore pressures. The plane strain analyses for $\omega=0^0$, 90^0 use a similar mesh of quadrilateral elements and similar interpolation.

Prior research on related analyses of cavity contraction problems in elasto-plastic soils (e.g., Ewy, 1993; Yu and Rowe, 1999) show that the predictions are strongly related to the constitutive behavior and stress-strain properties of the formation soils. The mechanical response of low permeability clays is highly complex and involves non-linear and inelastic behavior even at small levels of shear strain (as small as 10^{-3}%), while anisotropic stress-strain-strength properties are previously observed due to 1-D consolidation stress history. The current research compares predictions of stress conditions around wellbores using two effective stress soil models: 1) Modified Cam Clay (MCC); (Roscoe and Burland 1968); and 2) MIT-E3 (Whittle and Kavvadas 1994). The results using MCC serve as a base case, and are amenable to simplified interpretation due to model assumptions of isotropic yield and critical state. The current formulation of the MCC model assumes a constant elastic Poisson's ratio, ν', and uses an extended von Mises (Drucker-Prager) criterion to generalize the yield and failure surfaces. MIT-E3 is a more

complex model that is able to represent non-linear and anisotropic stress-strain properties observed in laboratory element tests.

It should be noted that both soil models assume normalized engineering properties of materials (Ladd and Foott 1974) such that stiffness and shear strength properties are proportional to σ'_{v0} at a given overconsolidation ratio, OCR ($=\sigma'_p/\sigma'_{v0}$). Casey and Germaine (2013) have recently shown that normalized properties are only valid over a relatively narrow range of vertical preconsolidation pressures, σ'_p. Hence, the current models must be calibrated to the specific range of consolidation pressures relevant to wellbore stability. In this study, the soil models are calibrated to results from a suite of laboratory experiments on the analog soil, Resedimented Boston Blue Clay. (RBBC; Abdulhadi et al. 2012). This material is considered a representative of non-reactive shale (I_p = 22.7 ± 1.2%). RBBC is prepared in the laboratory from powdered natural Boston Blue Clay, an illitic glacio-marine clay of low to medium sensitivity. Figure 4 illustrates the calibration of the MCC and MIT-E3 models from undrained triaxial shear tests performed with pre-consolidation pressure in the range, σ'_p= 1-10 MPa (corresponding to depths ranging from 100-1000m).

Tables 1 and 2 list the input parameters obtained from these calibrations. The following points can be noted from Figure 4:

1) The MIT-E3 model matches closely the effective stress-strain-strength properties measured in both triaxial extension and compression modes of shearing. Results in Figure 4b highlight the non-linearity of stress-strain behavior, while Figure 4a shows the shear-induced pore pressures (effective stress path) and frictional shear strength at large strains. There is a large difference in the undrained shear strength ratio of normally consolidated clay measured in the two shear modes (s_{uTC}/σ'_{vc} = 0.28 vs s_{uTE}/σ'_{vc} = 0.15).

2) The MCC model assumes that there is a unique undrained shear strength that is distinguished at large strains. The model provides a reasonable representation of shearing in triaxial compression but grossly overestimates the shear strength in triaxial extension due to the assumptions of isotropic yielding.

Akl and Whittle (2016) have made detailed evaluations of the constitutive model performance in interpreting the results of laboratory model borehole tests using Thick Walled Cylinder (TWC) tests (data reported by Abdulhadi et al. 2011). Figure 5 compares the computed and measured results of the volumetric strains inside the model wellbore due to depressurizing the internal cavity. The measured data show critical net pressure, $(p_i - u_0)/\sigma'_{vc} = 0.3 \pm 0.05$ for tests performed with consolidation stresses, σ'_{vc} = 1.5-10 MPa. The MIT-E3 model tends to underestimate the initial stiffness at the start of the tests (i.e. higher $\Delta V/V_0$ at a given internal pressure) but accurately describes the critical net pressure ratio and deformations at the wellbore. In contrast, MCC predicts that the wellbore remains stable at pressures well below the measured critical condition. These results highlight the predictive ability of MIT-E3 to describe deformations and stability of wellbores, while the assumptions of isotropic yield case in MCC to underestimate the volume strains (borehole closure) and overestimate wellbore stability.

UNDRAINED ANALYSIS OF WELLBORE STABILITY

The evaluation of wellbore stability is particularly problematic for a number of reasons: i) direct observation is impossible when the drill bit is thousands of meters away; ii) in situ stresses are not measured systematically; and iii) there can be large variations in the material properties. The complexity of the wellbore problem and the abundance of intertwined factors affecting

wellbore stability make comprehensive modeling a significant challenge. In complex processes such as these, for which parameters are ill-defined or excessively difficult to collect, parametric analyses provide a useful framework for understanding the stability mechanisms. The current analyses consider how changes in the mud weight affect wellbore deformations and stability. This is achieved by simulating the decrease in mud pressure within the wellbore.

Initially we assume that typical drilling rates are sufficiently rapid that there is little time for migration of pore fluid within the low permeability formation (Detournay and Cheng 1988), and hence the formation is sheared under undrained conditions. Pressures within the wellbore are reduced in two steps: 1) the deviatoric component of stresses at the cavity wall is relieved; and then 2) radial pressures are reduced until the critical pressure where uncontrolled deformations occur. The current analyses define failure using one of two criteria: 1) failure occurs due to instability in the stress field producing large localized deformations (cf. Effect of wellbore inclination) at points around the wellbore; or 2) there are large uniform cavity deformations corresponding to $\delta_{cr}/R_0 = 0.1$ (10%), where 'cr' is a reference to the 'crown point' on the perimeter of the wellbore (i.e., the point at the highest elevation). The latter case corresponds to excessive squeezing of the formation that could restrict installation of the casing.

Effect of wellbore inclination

Figures 6a and 6b show inward deformations of the wellbore as a function of the net total radial stress ratio acting at the crown point, $(\sigma_{rr}-u_0)/\sigma'_{v0,}$ where u_0 and σ'_{v0} are the in situ pore pressure and the vertical effective stress in the formation for wellbores at 5 different inclination angles in K_0-normally consolidated RBBC. Results from the MCC model (Fig. 6a) show that the wellbore is stable well below the underbalanced mud pressure (i.e., $(\sigma_{rr}-u_0)/\sigma'_{v0}= 0$) for all

wellbore inclinations, while failure due to excessive cavity deformations ($\delta_{cr}/R_0 \geq 10\%$) at ($\sigma_{rr}$-$u_0$)/$\sigma'_{v0} \approx$ -0.7 to -0.9 (i.e. there is no tendency for localized failure modes).

In contrast, results for the MIT-E3, Figure 6b, show localized failures for all deviated wellbores ($\omega > 0^0$). Highly deviated wellbores ($\omega \geq 45^0$, Fig. 6b) fail at pressures above the underbalanced drilling limit (i.e., (σ_{rr}-u_0)/$\sigma'_{v0} \geq 0$) at crown displacements, $\delta_{cr}/R_0 \leq 0.05$. Only the vertical wellbore reaches the failure criterion for excessive wall deformation (at (σ_{rr}-u_0)/σ'_{v0} = -0.32).

For vertical wellbores, both MIT-E3 and MCC soil models predict large plastic deformations at mud pressures far below the underbalanced drilling limit (-0.32σ'_{v0} and -0.95σ'_{v0}, respectively). This case can occur as unplanned blowout (kick) events in wells as reported by Willson et al. (2013), who argue that in ductile formations the kick-induced collapse can be considered as a bridging procedure that mitigates the blowout.

Figures 7a and 7b illustrate the deformed shapes of the wellbore cavities computed at failure (using the undeformed cavity as a datum) for the same 5 wellbore inclinations using the MCC and MIT-E3 models, respectively. The MCC model predicts regular oval-shaped cavity for inclined wellbores elongated along the local y-axis as shown in Figure 7a. The inward deformation at the reference crown point is 10% at failure for all wellbores according to the second failure criterion. The inward deformation at the springline increases with the deviation angle. The distortion ratios increase with the deviation angle, (δ_{sp}/δ_{cr} = 1.09 at $\omega = 30^0$ to 1.3 at $\omega = 90^0$).

In contrast, MIT-E3 generates irregular deformation modes around the cavity for all deviated wellbores, Figure 7b. The $\omega = 30^0$ case shows local inward deformation at crown point (8%) and

springline (9.8%), while $\omega = 45^0$ and 60^0 show larger deformations near the springline (4.5%). The inward deformation for 90^0 wellbore (horizontal wellbore) at the crown point reaches 2.8% but the maximum deformations occurs locally at $\theta=15^0$, where δ_r =3.1%. These results all indicate the onset of local failure mechanisms in the formation.

Further insights in the failure mechanisms for the MIT-E3 analyses can be obtained by considering the equivalent shear strains, |E| predicted within the formation. Figure 8 shows the distribution of the shear strains around vertical and deviated wells at a 'reference state' with $(\sigma_{rr}-u_0)/\sigma'_{v0}$ =0.2 (cf. Fig. 6). At this reference mud pressure ratio, the equivalent shear strains increase at the cavity wall with the deviation angle of the wellbore; and the zone of influence ($|E| \geq 0.1\%$) extends further into the formation at lobe angles ranging from $\theta=45^0$ - 53^0 ($\omega=30^0$ and 60^0, respectively). At failure, large shear strains ($|E| \geq 10\%$) occur close to the wellbore but their distribution is strongly affected by the deviation angle. Failure occurs when shear strains increase at the crown point and springline (Fig. 8d). The small zones of high shear strains at $\theta=0^0$ and 90^0 are linked to the excessive local deformations presented in Figure 7b. The shear strains around the 45^0 (Fig. 8f) and 60^0 (Fig. 8h) deviated wells increase at the cavity wall within the range of $\theta=0^0$ to 20^0 with decrease in mud pressure. When zones of high shear strains are formed at the springline point; distortions and excessive inward deformations lead to failure.

Figures 8i and 8j show the shear strains around the horizontal wellbore. High shear strains up to 27% develop at $\theta=15^0$ where local increase in inward deformations occurs as shown in Figure7b. The propagation of large shear strains into the formation is indicative of the tendency to form a breakout around the springline of the wellbore.

Effect of Stress History

The effects of stress history can be interpreted by considering the overconsolidation ratio, OCR = σ'_p/σ'_{v0} of the clay. Undrained strength ratio and normalized secant stiffness modulus increase with overconsolidation ratio of RBBC as shown in many element shear tests in the lab (e.g., Ladd and Varallyay 1965). Table 3 shows the MIT-E3 predictions of RBBC undrained shear strength and stiffness at different OCR values. Figure 9 shows horizontal wellbore inward deformations as a function of net total radial stress ratio, $(\sigma_{rr}-u_0)/\sigma'_{v0}$ for OCR =1.0-4.0. MIT-E3 model predicts early failure in horizontal wells in normally consolidated RBBC $(\sigma_{rr}-u_0)/\sigma'_{v0}$ = 0.18 shown previously in Fig. 6b. At OCR=1.5, the wellbore is stable at mud pressures below the underbalanced drilling limit. At higher OCR values, the required mud pressure ratio to prevent failure (net critical mud pressure ratio) decreases to $-0.25\sigma'_{v0}$, $-0.49\sigma'_{v0}$ and $-1.26\sigma'_{vc}$ for OCR=1.5, 2.0 and 4.0 respectively. Failure also occurs due to local increases in deformations and high shear strains (as described above for the NC clay).

CONSOLIDATION ANALYSIS OF WELLBORE STABILITY

In practice the wellbore is stabilized by steel casings that are typically installed a relatively short time after drilling. If there are delays in the casing installation, consolidation within the formation (i.e. migration of pore fluid) can also affect wellbore stability. These effects are examined by further numerical analyses of coupled time-dependent deformations and pore pressures referred to as E-C coupled consolidation (Whittle et al. 2001). These analyses use the same effective stress soil models, while seepage of pore water is controlled by Darcy's law with hydraulic conductivity controlled by the current void ratio of the formation. Pore pressure

migration and redistribution occur in the same plane as the formation deformations. In all cases we assume undrained conditions for initial wellbore drilling, and focus on a reference stable mud pressure, $(\sigma_{rr} - u_0)/\sigma'_{v0} = 0.2$, Figure 10. We then consider changes in wellbore stability due to coupled consolidation (deformations and flow) over a period of 30 days (i.e., one month delay for casing installation). Following Whittle et al. (2001) the consolidation can be characterized by a dimensionless time factor:

$$T = \frac{\sigma'_p k t}{\gamma_w R^2} \quad (1)$$

where t is the time after undrained unloading occurred, σ'_p is the vertical pre-consolidation pressure, k is the hydraulic conductivity, R the cavity radius, and γ_w the unit weight of water.

In practice drainage boundary conditions at the wellbore are not well controlled. The current analyses consider two limiting cases: 1) The wellbore is permeable (i.e., the filter cake is ineffective) and the formation pore pressures equilibrate to wellbore mud pressures; and 2) The wellbore is impermeable (i.e., a perfect filter cake sealing the cavity wall), and there is no fluid flux into the cavity. Figure 10 illustrates MIT-E3 predictions of excess pore pressure distributions $(\Delta u/\sigma'_{v0})$ for the two cases around a horizontal wellbore and shows how the cavity boundary conditions drive the redistribution of the pore pressures in the formation around the wellbore.

The boundary condition is:

Impermeable case: $$\left.\frac{\partial u}{\partial r}\right|_{R_0} = 0 \quad (2)$$

Permeable case: $$\Delta u/\sigma'_{v0} = (\sigma_{rr} - u_0)/\sigma'_{v0} \quad (3)$$

Figures 11 a and b show change in the deformed shape of the wellbore cavity due to pore pressure redistribution around vertical and horizontal wellbores using the MIT-E3 soil model. For the vertical wellbore (Fig. 11a), the analyses show small inward deformations for both impermeable and permeable wellbore boundary conditions. For horizontal and other deviated wellbores ($\omega \neq 0^0$) there are significant gradients in excess pore pressure around the cavity (cf. Fig. 10). Subsequent consolidation computed for the horizontal wellbore (Fig. 11b), is accompanied by significant increases in the equivalent shear strains. Figures 11c and 11d show the possibility of a localized breakout developing around the springline of the wellbore with consolidation at constant mud pressure.

Figures 12a and 12b summarize the computed maximum cavity deformations occurring with time for the permeable and impermeable wellbores, respectively. The figures show that rate of inward deformations generally decrease with time and are more significant when there is a flux into the wellbore (permeable boundary). The figures also demonstrate that undrained deformations due to drilling (at T = 0, Fig. 11), are generally much larger than the subsequent consolidation-induced movements (for $T \leq 1.6$). Incremental changes in cavity displacement range from 11% to 70% for vertical and horizontal wellbores (Fig. 12a).

CONCLUSIONS

This paper presents numerical simulations of deviated wellbore deformations and stability in K_0-consolidated formations. The results highlight the importance of undrained formation

deformations during the drilling phase (under controlled mud pressures). Failure can occur due to localized failure modes (breakouts) or large uniform plastic deformations around the cavity wall. Smaller deformations can occur prior to casing installation due to coupled consolidation within the formation. These can contribute to instability and distortion of the wellbore depending on prior levels of mud pressure and deviation angle.

The main conclusions from the simulation are as follows

1. The complex behavior of unlithified formations affects its response to drilling wellbores and requires a realistic model to assess stability mechanisms of such wellbores. The current study shows predictive capabilities of the MIT-E3 with TWC tests. Predictions for deviated wellbores using MIT-E3 show that mud pressures must be maintained well above the underbalanced drilling limit (up to $(\sigma_{rr} - u_0)/\sigma'_{v0} = 0.2$) to prevent localized failures during drilling for horizontal and highly deviated wellbores.
2. Consolidation within the formation generally produces smaller deformations of the wellbore cavity compared to undrained drilling (from 0% for the impermeable vertical wellbore to 70% for the permeable horizontal wellbore). Incremental cavity deformations depend on drainage conditions at the cavity wall and wellbore deviation. However, if high shear strains occur in the formation during drilling, localized failure can develop in deviated wellbores over time as consolidation induces localized breakout mechanisms.

ACKNOWLEDGMENTS

This research was sponsored by BP America., Houston, and by the BP-MIT Major Projects Program. The authors are grateful for Dr. Stephen Willson for his technical advice and support.

REFERENCES

Abdulhadi, N. O., Germaine, J. T., and Whittle, A. J. 2011. "Experimental study of wellbore instability in clays." *Journal of Geotechnical and Geoenvironmental Engineering*, 137(8), 766-776.

Abdulhadi, N. O., Germaine, J. T., and Whittle, A. J. 2012. "Stress-dependent behavior of saturated clay." *Canadian Geotechnical Journal*, 49(8), 907-916.

Akl, S. A. 2010. "Wellbore Instability Mechanisms in Clays." PhD thesis, Dept. of Civil and Environmental Engineering, MIT, Cambridge, MA.

Akl, S. A. Y. and Whittle, A. J. 2016. "Validation of soil models for wellbore stability in ductile formations using laboratory TWC tests." *To appear ASCE Journal of Geotechnical and Geoenvironmental Engineering.*

Casey, B., and Germaine, J. T. 2013. "Stress dependence of shear strength in fine-grained soils and correlations with liquid limit." *Journal of Geotechnical and Geoenvironmental Engineering*, 139(10), 1709-1717.

Charlez, Ph., and Heugas, O. 1991. "Evaluation of Optimal Mud Weight in soft shale levels", *Rock Mechanics as a Multidisciplinary Science* (Editor: Roegiers), Balkema, 1005-1014.

Detournay, E. and Cheng, A. 1988. "Poroelastic response of a borehole in a non-hydrostatic stress fields", *International journal of Rock Mechanics and Mining sciences and Geomechanics Abstracts*, 25, 255-266.

Ewy, R. T. 1993. "Yield and Closure of Directional and Horizontal Wells", *International Journal of Rock Mechanics, Mining Sciences, and Geomechanics Abstracts*, 30(7), 1061-1067.

Fjaer, E., Holt, R.M., Horsrud, R., Raaen, A.M., and Risnes, R. 2008 *Petroleum Related Rock Mechanics*, 2nd Edition, Elsevier.

Hibbett, Karlsson, & Sorensen Inc. 1998. ABAQUS/Standard: User's Manual (Vol. 1). Hibbitt, Karlsson & Sorensen, Inc.

Ladd, C. C. and Varallyay, J. 1965. "The influence of stress system on the behavior of saturated clays during undrained shear," Research Report R65-11, Soil Publication No. 1777, Department of Civil Engineering, MIT, Cambridge, MA.

Ladd, C.C., and Foott, R. 1974. "New design procedure for stability of soft clays." ASCE Journal of the Geotechnical Engineering Division, 100(7), 763–786.

Roscoe, K.H., and Burland, J.B. 1968. "On the generalized stress-strain behavior of 'Wet' clay." In *Engineering Plasticity*, Ed. J. Heyman and Leckie, F. A. Cambridge University Press, 535-609.

Santarelli, F.J., Brown, E.T. and Maury, V. 1986. "Analysis of borehole stressing using pressure-dependent, linear elasticity." *International Journal for Rock Mechanics and Mining Sciences*, 23(6), 445-449.

Whittle, A.J., and Kavvadas, M. 1994. "Formulation of the MIT-E3 Constitutive Model for Overconsolidated Clays." *ASCE Journal of Geotechnical Engineering*, 120 (1), 173-198.

Whittle, A.J., Sutabutr, T., Germaine, J.T., and Varney, A. 2001. "Prediction and interpretation of pore pressure dissipation for a tapered piezoprobe." *Géotechnique*, 51(7), 601-617.

Willson, S.M., Nagoo, A.S., and Sharma, M.M. 2013. "Analysis of Potential Bridging Scenarios During Blowout Events." In *SPE/IADC Drilling Conference*. Society of Petroleum Engineers.

Yu, H., and Rowe, R. K. 1999. "Plasticity Solutions for Soil Behavior around Contracting Cavities and Tunnels." *International Journal for Numerical and Analytical Methods in Geomechanics*, 23, 1245-1279.

APPENDIX A: Transformation of Geostatic Stress Tensor under Frame Rotation

$$[\sigma_{local}] = [R]^T[\sigma_{global}][R]$$

where:

$$[\sigma_{global}] = \begin{bmatrix} \sigma'_{XX} & \sigma'_{XY} & \sigma'_{XZ} \\ \sigma'_{XY} & \sigma'_{YY} & \sigma'_{YZ} \\ \sigma'_{XZ} & \sigma'_{YZ} & \sigma'_{ZZ} \end{bmatrix} = \begin{bmatrix} K_0\sigma'_{v0} & 0 & 0 \\ 0 & \sigma'_{v0} & 0 \\ 0 & 0 & K_0\sigma'_{v0} \end{bmatrix}$$

$$[R] = \begin{bmatrix} 1 & 0 & 0 \\ 0 & \cos\omega & \sin\omega \\ 0 & -\sin\omega & \cos\omega \end{bmatrix}$$

$$[\sigma_{local}] = \begin{bmatrix} K_0\sigma'_{v0} & 0 & 0 \\ 0 & \sigma'_{v0}\cos^2\omega + K_0\sigma'_{v0}\sin^2\omega & \sigma'_{v0}\cos\omega\sin\omega - K_0\sigma'_{v0}\sin\omega\cos\omega \\ 0 & \sigma'_{v0}\sin\omega\cos\omega - K_0\sigma'_{v0}\sin\omega\cos\omega & \sigma'_{v0}\sin^2\omega + K_0\sigma'_{v0}\cos^2\omega \end{bmatrix}$$

List of Figure Captions

Figure 1 Schematic diagram showing the wellbore mechanical model with respect to the global (X, Y, Z) and local (x, y, z) frames of reference

Figure 2 A schematic diagram showing the far field stresses for the general and special cases of wellbores in the plane of analysis orthogonal to the wellbore axis, z.

Figure 3 Schematic diagrams showing the finite element mesh used for the quasi 3D wellbore problem and a sketch of the 3D brick elements used in the mesh.

Figure 4 Calibration of the MIT-E3 and MCC material models with high pressure triaxial compression and extension tests performed on RBBC (Akl 2010).

Figure 5 Comparison between measured behavior of model wellbore and numerical simulations using MIT-E3 and MCC soil models (Akl 2010).

Figure 6 Effect of Wellbore Inclination on Computed pressure-deformation at wellbore in K_0-normally consolidated RBBC for two effective stress soil models.

Figure 7 Radial deformations at critical mud pressures computed by two effective stress soil models at cavity wall for vertical and deviated wellbores. (Deformations are scaled 5:1)

Figure 8 Equivalent shear strain, $|E|^*$ contours computed by MIT-E3 model for wellbores with 5 different inclinations, where |E| is the second invariant of the shear strain tensor.

*$|E|=\sqrt{E_i E_i}$, where i=1-5, equation from (Whittle and Kavvadas 1994).

Figure 9 Effects of stress history on relationship between wellbore deformations and radial stresses at cavity wall for a horizontal wellbore ($\omega=90^0$) in K_0-consolidated RBBC.

Figure 10 Conceptual figure showing consolidation after undrained excavation of wellbore where $\Delta u/\sigma'_{v0}$ are the excess pore pressures.

Figure 11 Effect of coupled consolidation on stability of vertical (a) and horizontal wellbores (b-d) from MIT-E3 simulations in K_0-normally consolidated RBBC formation.

Figure 12 Effect of consolidation on cavity maximum inward deformations of deviated wellbores for permeable and impermeable wellbores.

List of Table Captions

Table 1 Input parameters for the MCC model (Akl, 2010).

Table 2 Input parameters for the MIT-E3 model (Akl, 2010).

Table 3 MIT-E3 predictions of RBBC engineering properties at different OCR values.

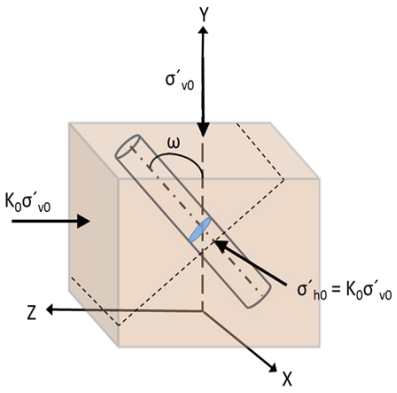

a) Wellbore deviation, global reference frame

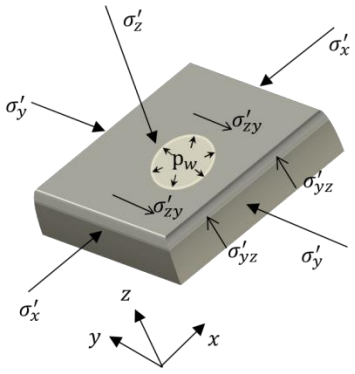

b) stress conditions, local reference frame

Figure 1 Schematic diagram showing the wellbore mechanical model with respect to the global (X, Y, Z) and local (x, y, z) frames of reference

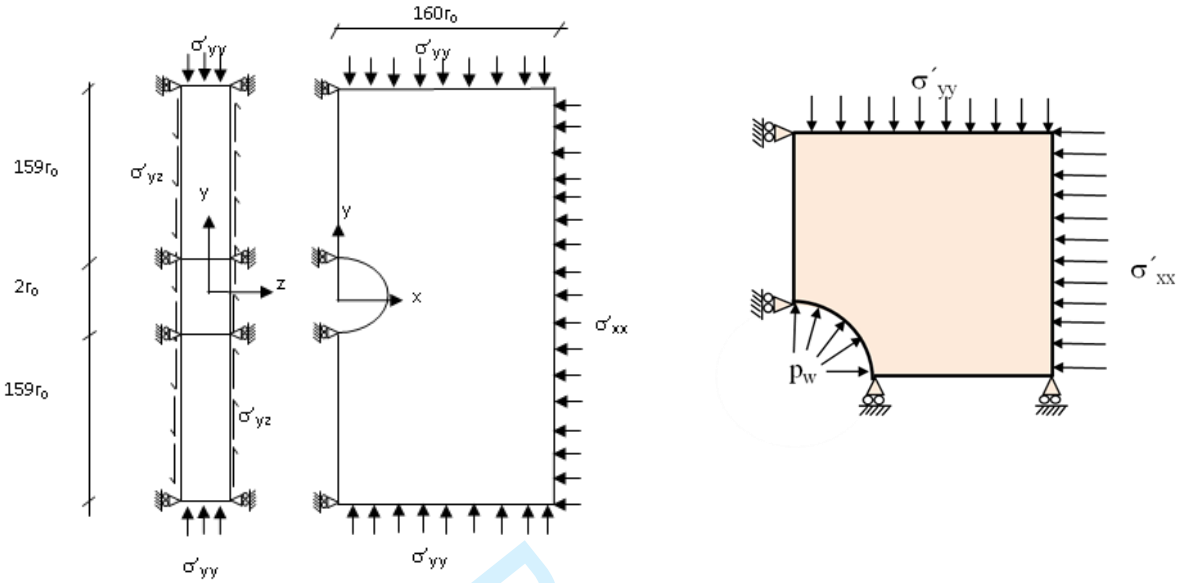

a) Slice model, quasi -3D structure for deviated wellbores

b) plane strain geometry of of vertical and horizontal wellbores.

Figure 2 A schematic diagram showing the far field stresses for the general and special cases of wellbores in the plane of analysis orthogonal to the wellbore axis, z.

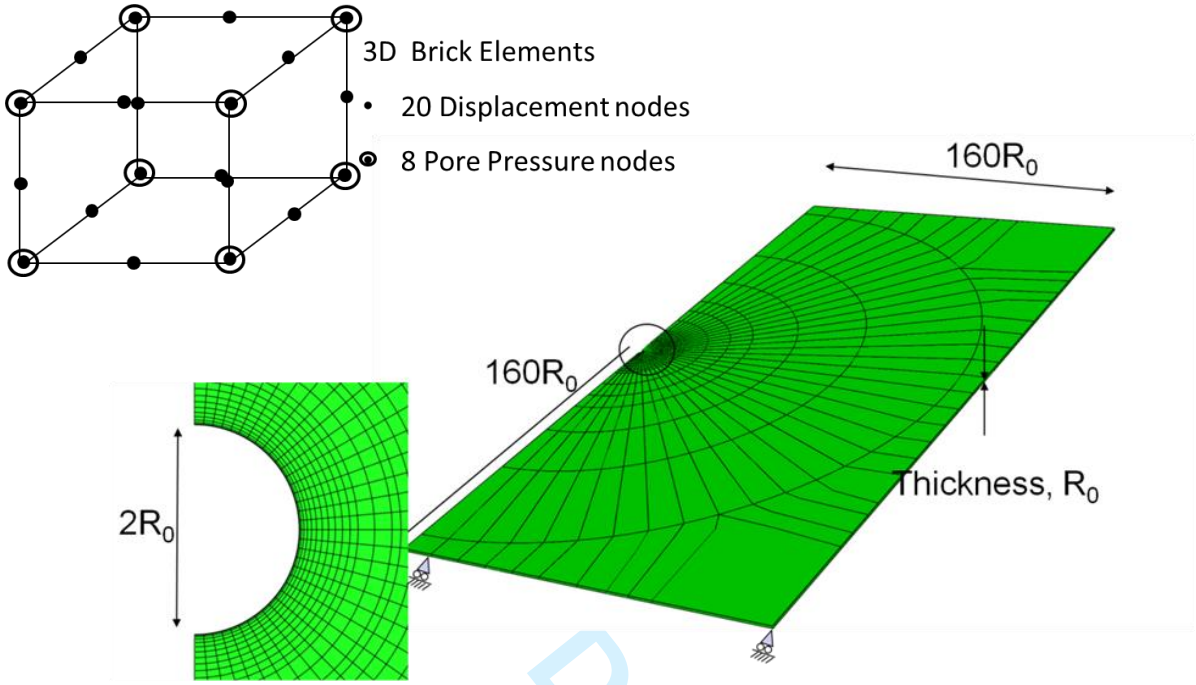

Figure 3 Schematic diagrams showing the finite element mesh used for the quasi 3D wellbore problem and a sketch of the 3D brick elements used in the mesh.

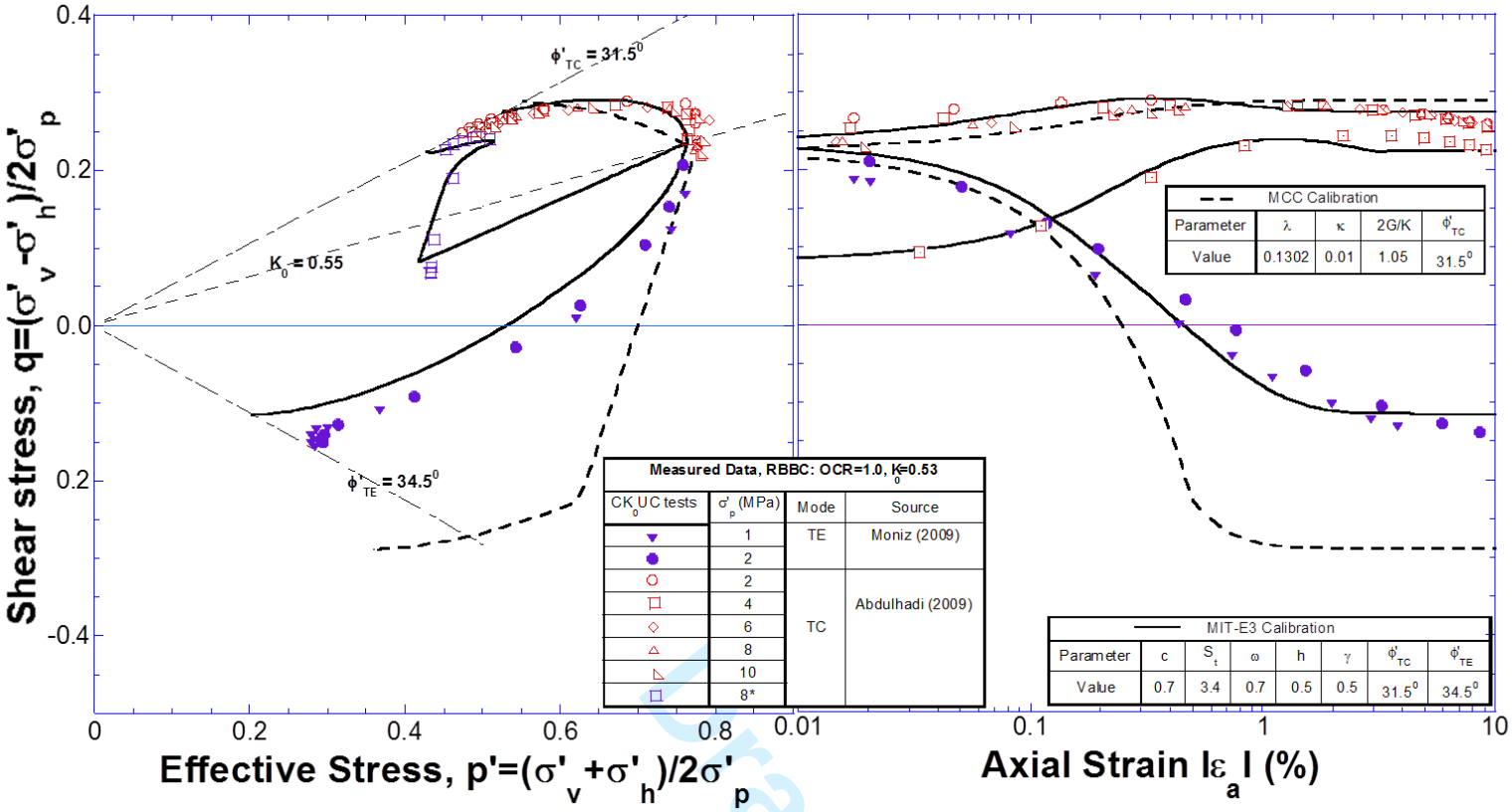

*Note: OCR = 2.0

Figure 4 Calibration of the MIT-E3 and MCC material models with high pressure triaxial compression and extension tests performed on RBBC (Akl 2010).

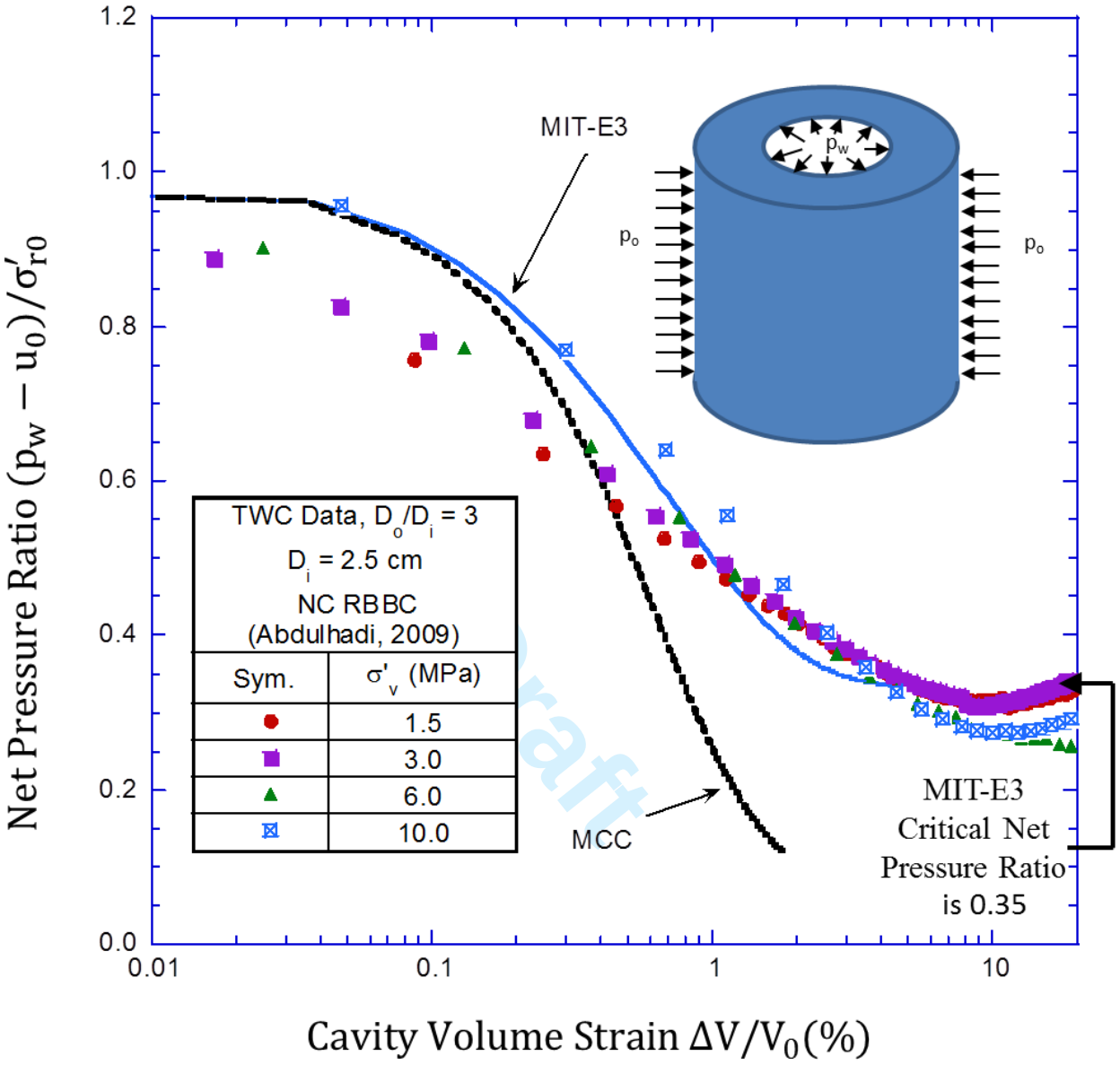

Figure 5 Comparison between measured behavior of model wellbore and numerical simulations using MIT-E3 and MCC soil models (Akl 2010).

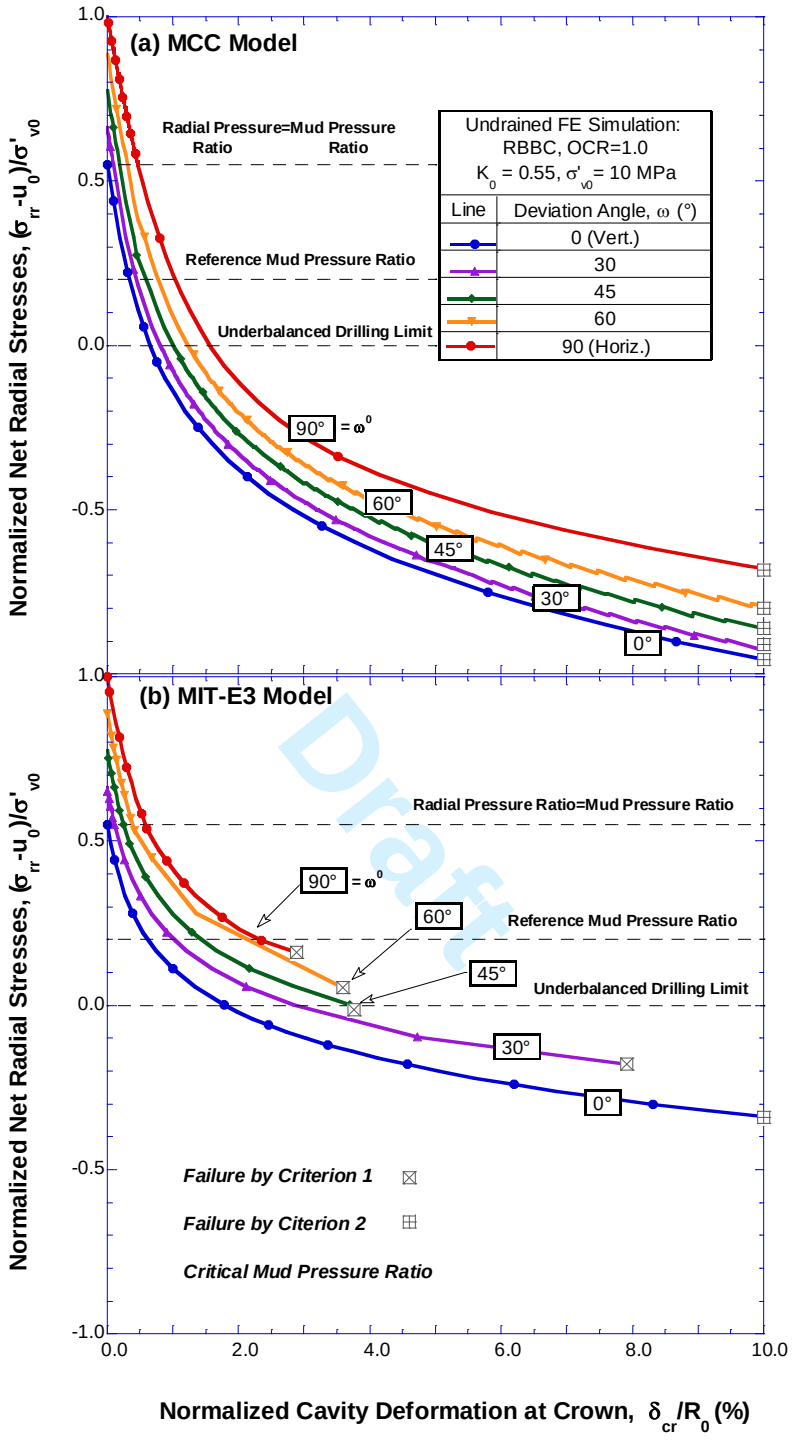

Figure 6 Effect of Wellbore Inclination on Computed pressure-deformation at wellbore in K_0-normally consolidated RBBC for two effective stress soil models.

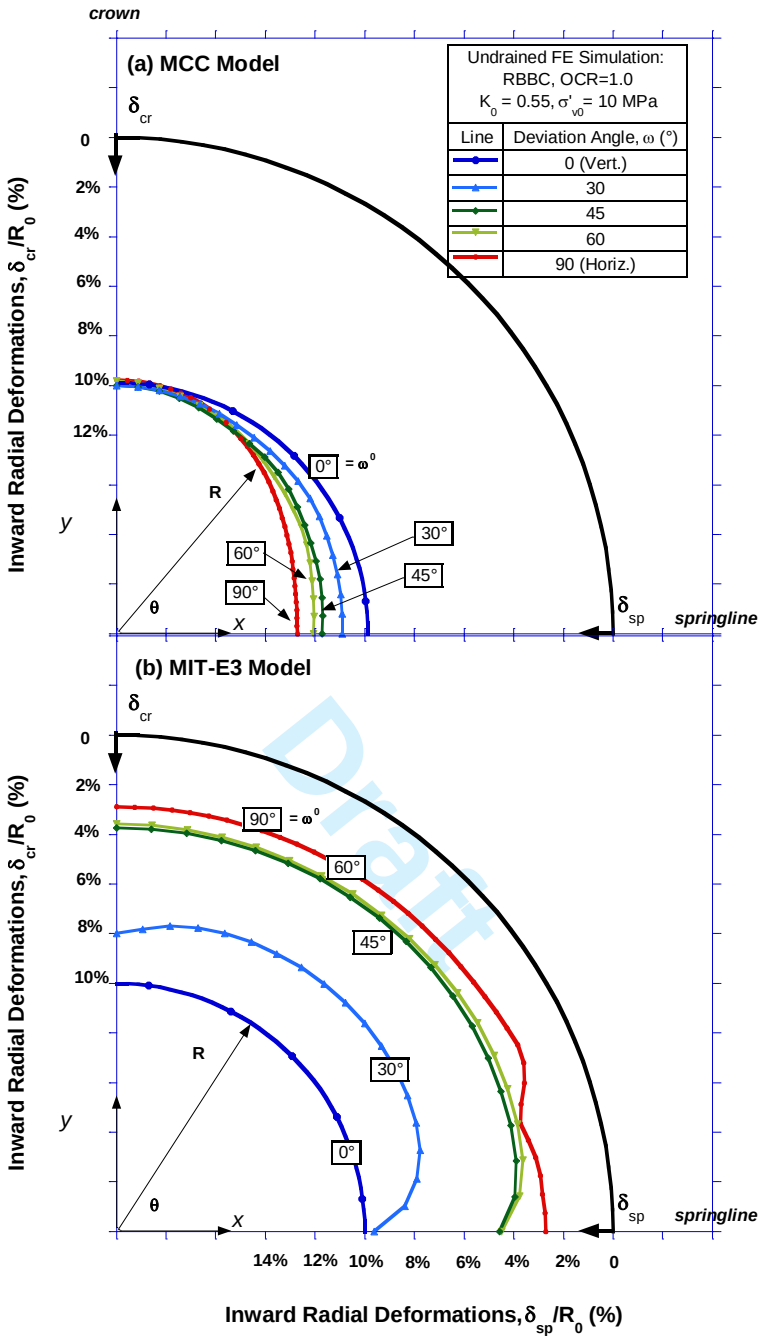

Figure 7 Radial deformations at critical mud pressures computed by two effective stress soil models at cavity wall for vertical and deviated wellbores. (Deformations are scaled 5:1)

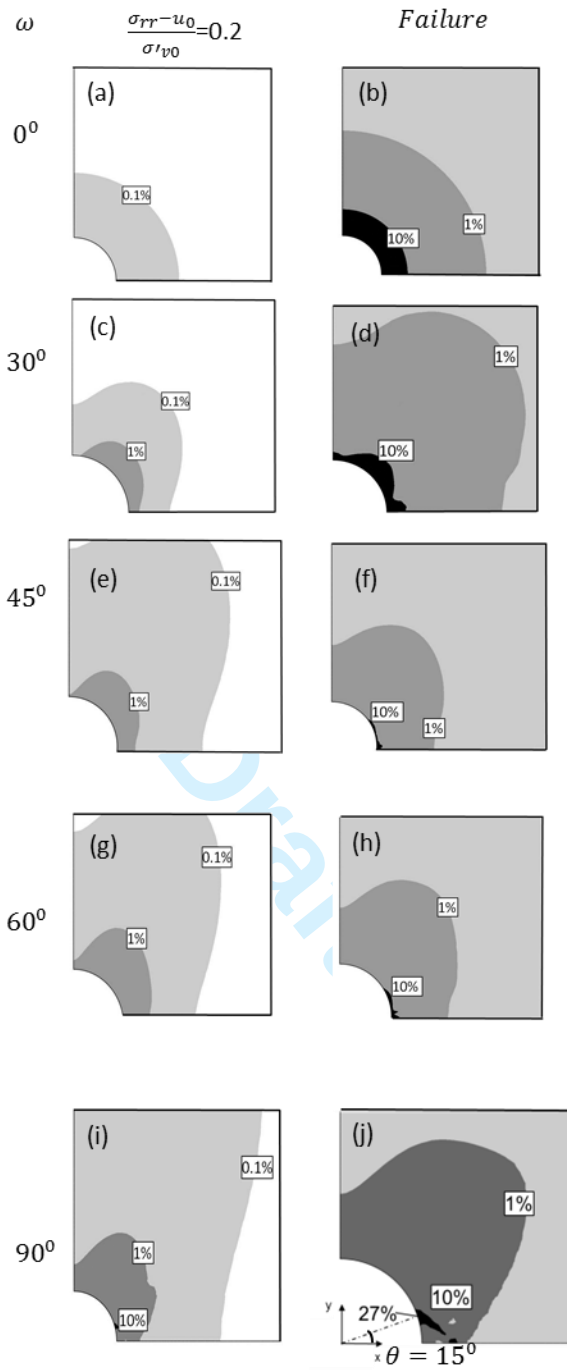

Figure 8 Equivalent shear strain, $|E|^*$ contours computed by MIT-E3 model for wellbores with 5 different inclinations, where |E| is the second invariant of the shear strain tensor.

*$|E|=\sqrt{E_i E_i}$, where i=1-5, equation from (Whittle and Kavvadas 1994).

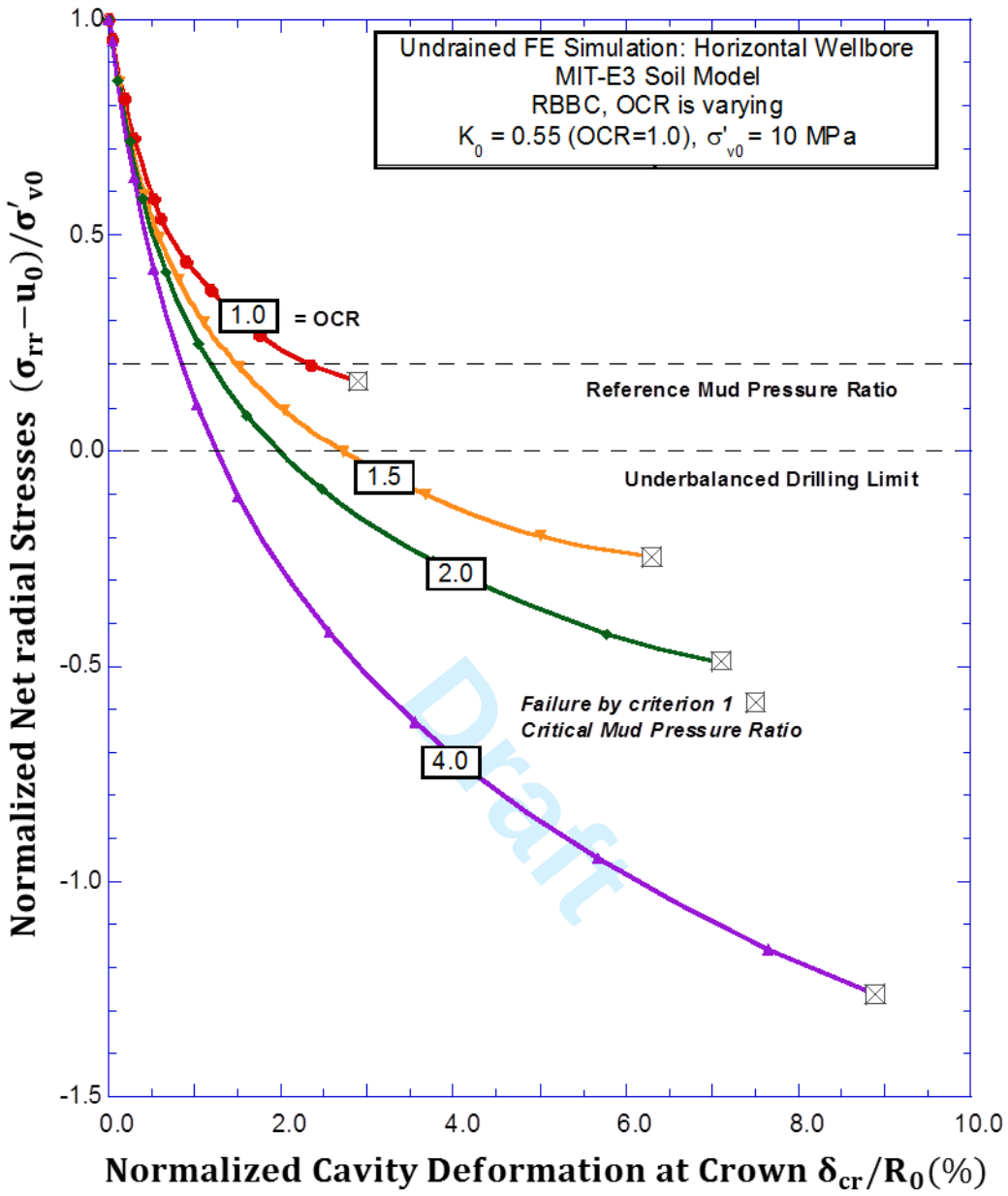

Figure 9 Effects of stress history on relationship between wellbore deformations and radial stresses at cavity wall for a horizontal wellbore ($\omega=90^0$) in K_0-consolidated RBBC.

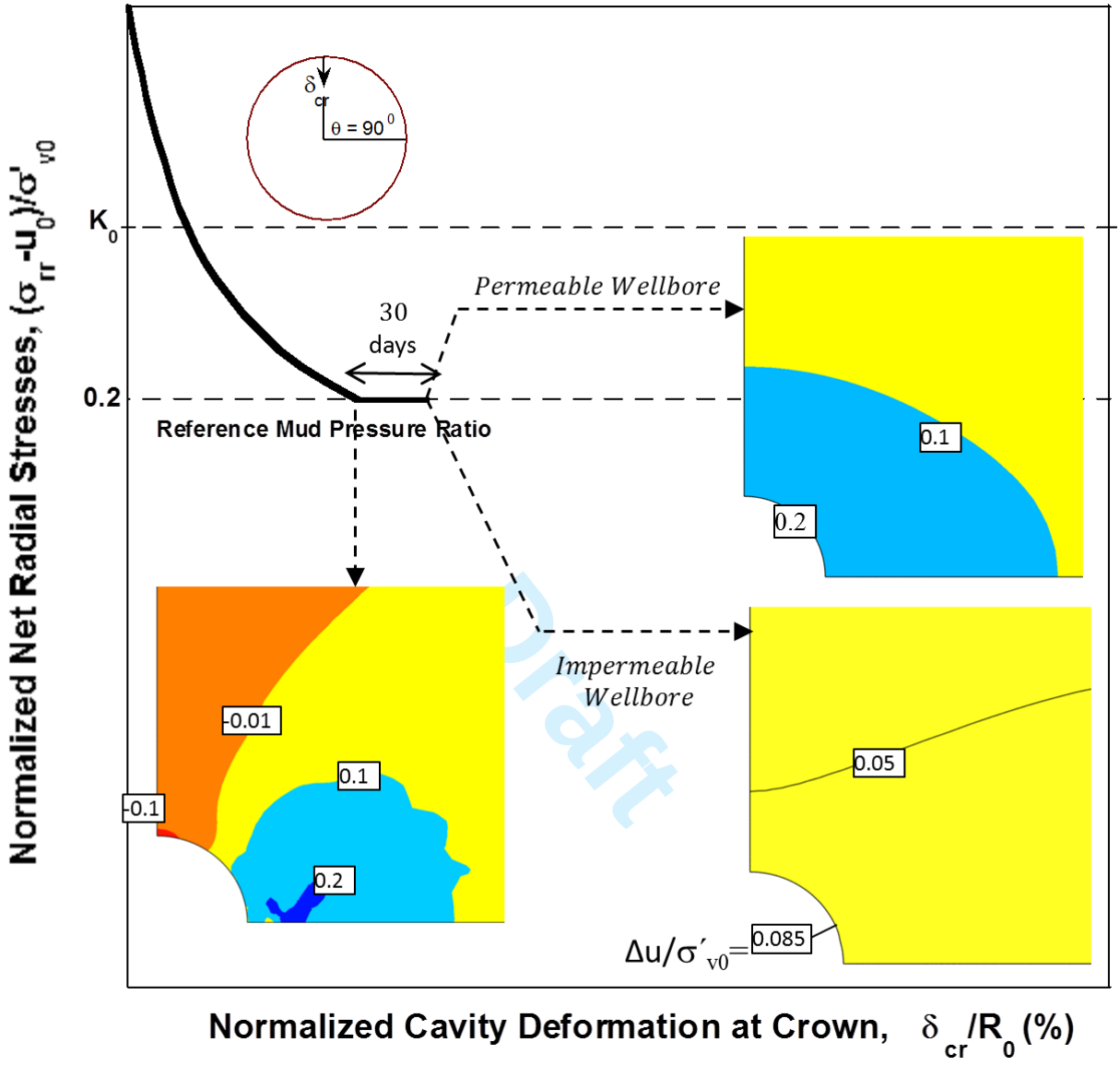

Figure 10 Conceptual figure showing consolidation after undrained excavation of wellbore where $\Delta u/\sigma'_{v0}$ are the excess pore pressures.

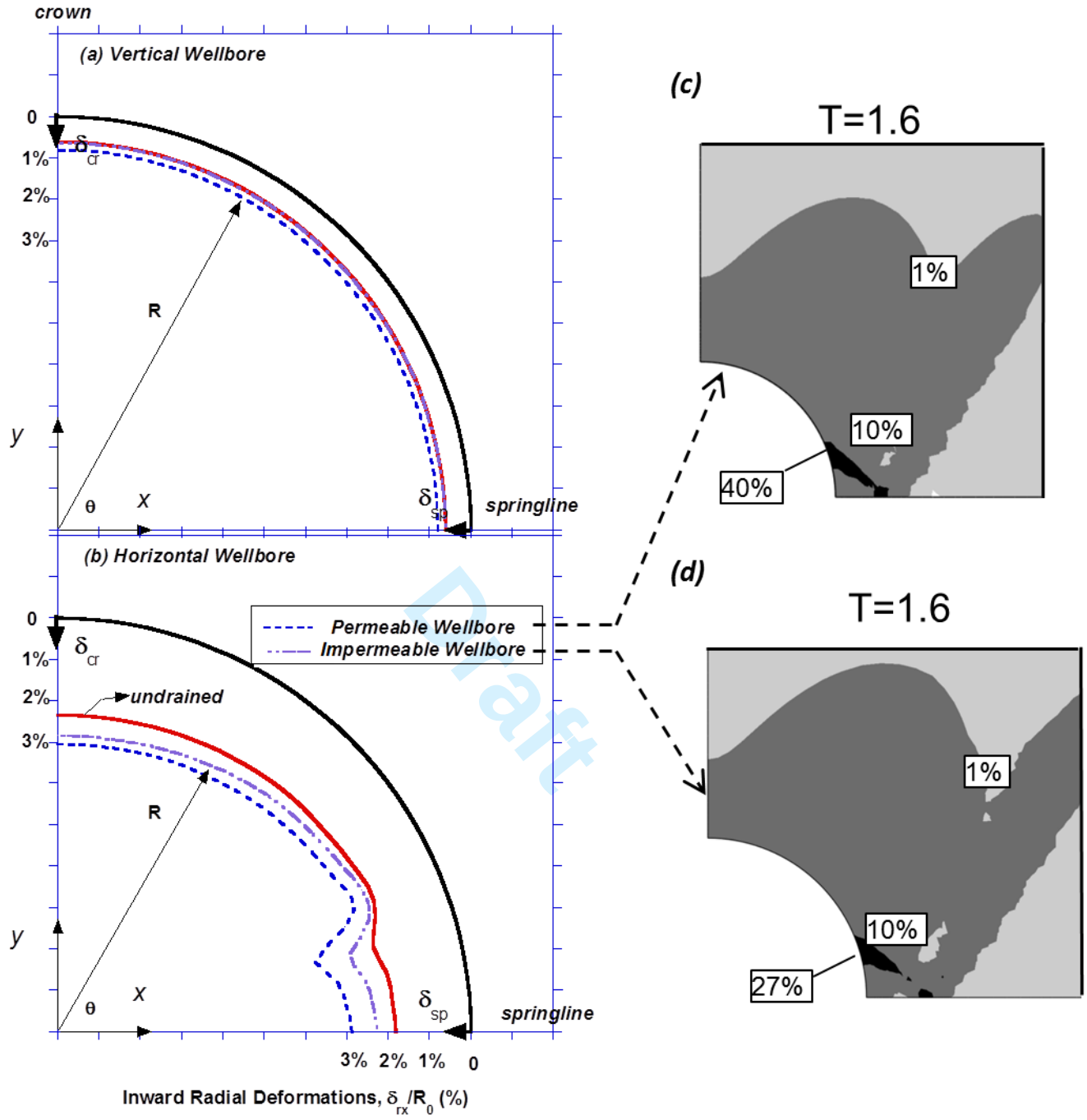

Figure 11 Effect of coupled consolidation on stability of vertical (a) and horizontal wellbores (b-d) from MIT-E3 simulations in K_0-normally consolidated RBBC formation.

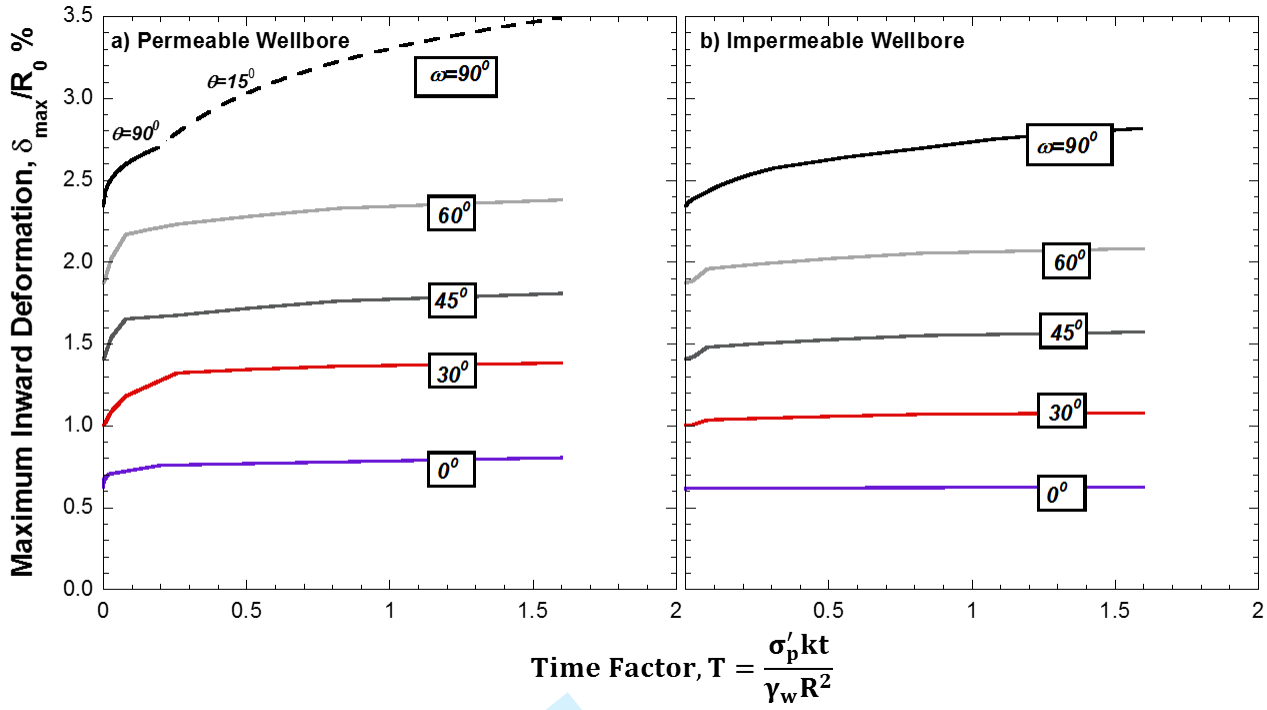

Figure 12 Effect of consolidation on cavity maximum inward deformations of deviated wellbores for permeable and impermeable wellbores.

Table 1 Input parameters for the MCC model (Akl, 2010).

Laboratory Test	Description	Parameter	Calibrated Value
One-dimensional Compression	Initial void ratio	e_0	0.65
	Compression Coefficient	λ	0.130
	Swelling Coefficient	κ	0.01*
	Poisson's Ratio	2G/K	1.05
Undrained Triaxial	Critical State Friction Angle	ϕ'_{TC}	31.5^0

*Calibrated to match $G_{0.01\%}/\sigma'_{vc}$ in CK_0UC test.

Table 2 Input parameters for the MIT-E3 model (Akl, 2010).

Laboratory Test	Description	Parameter	Calibrated Value
One-dimensional Compression	Initial Void Ratio	e_0	0.65
	Compression Coefficient	λ	0.1302
	Volumetric Swelling Behavior	C	1.0
		n	1.05
	Irrecoverable Plastic Strain	h	0.5
K_0 –oedometer or K_0 -Triaxial	K_0 for virgin normally consolidated clay	K_{0NC}	0.55
	Poisson's Ratio	2G/K	1.05
Undrained Triaxial Shear Tests OCR=1; CK_0UC OCR=1; CK_0UE OCR=2; CK_0UC	Critical State Friction Angles in Triaxial Compression and Extension	ϕ'_{TC}	31.5^0
		ϕ'_{TE}	34.5^0
	Undrained Shear Strength (geometry of bounding surface)	c	0.7
	Amount of Post-peak Strain Softening in Undrained Triaxial Compression	S_t	3.4
	Non-linearity at Small Strains in Undrained Shear	ω	0.7
	Shear Induced Pore Pressures for OC Clay	γ	0.5
Shear Wave Velocity	Small strain compressibility at load Reversal	κ_0	0.006
Drained Triaxial	Rate of Evolution of Anisotropy (rotation of bounding surface)	ψ_0	100
CRS	Hydraulic Conductivity	k^* cm/sec	$7x10^{-8}$

*Data from Abdulhadi (2009)

1 Table 3 MIT-E3 predictions of RBBC engineering properties at different OCR values.

OCR	K_0	Compression		Extension	
		s_{uTC}/σ'_{v0}	$G_{0.01\%}/\sigma'_{v0}$	s_{uTE}/σ'_{v0}	$G_{0.01\%}/\sigma'_{v0}$
1.0	0.55	0.28	53	0.13	65
1.5	0.63	0.38	71	0.16	71
2.0	0.72	0.47	76	0.20	76
4.0	1.05	0.89	98	0.35	94

2